



## A DISCRETE MODEL FOR GEOMETRICALLY NONLINEAR FREE AND FORCED VIBRATIONS OF STEPPED AND CONTINUOUSLY SEGMENTED EULER-BERNOULLI AFG BEAMS (SAFGB) CARRYING POINT MASSES

Anass MOUKHLISS <sup>1,\*</sup>, Abdellatif RAHMOUNI <sup>2</sup>, Othman BOUKSOUR <sup>2</sup>, Rhali BENAMAR <sup>3</sup>

<sup>1</sup> National Higher School of Electricity and Mechanics, ENSEM, Hassan II University of Casablanca, B.P 8118 Oasis, Casablanca, Morocco

<sup>2</sup> Laboratory of Mechanics, Production and Industrial Engineering, LMPGI, Higher School of Technology of Casablanca, ESTC, Hassan II University of Casablanca, B.P 8112 Oasis, Casablanca, Morocco

<sup>3</sup> Laboratoire des Etudes et Recherches en Simulation, Instrumentation et Mesures LERSIM, Mohammed V University of Rabat-Mohammadia School of Engineering, Avenue Ibn Sina, Morocco

\* Corresponding author, e-mail: [anass.moukhliss@ensem.ac.ma](mailto:anass.moukhliss@ensem.ac.ma)

### Abstract

A discrete model is applied to handle the geometrically nonlinear free and forced vibrations of beams consisting of several different segments whose mechanical characteristics vary in the length direction and contain multiple point masses located at different positions. The beam is presented by an N degree of freedom system (N-Dof). An approach based on Hamilton's principle and spectral analysis is applied, leading to a nonlinear algebraic system. A change of basis from the displacement basis to the modal basis has been performed. The mechanical behavior of the N-Dof system is described in terms of the mass tensor  $m_{ij}$ , the linear stiffness tensor  $k_{ij}$ , and the nonlinear stiffness tensor  $b_{ijkl}$ . The nonlinear vibration frequencies as functions of the amplitude of the associated vibrations in the free and forced cases are predicted using the single mode approach. Once the formulation is established, several applications are considered in this study. Different parameters control the frequency-amplitude dependence curve: the laws that describe the variation of the mechanical properties along the beam length, the number of added masses, the magnitude of excitation force, and so on. Comparisons are made to show the reliability and applicability of this model to non-uniform and non-homogeneous beams in free and forced cases.

Keywords: discrete model, stepped beam, free and forced non-linear vibration, AFG beam, point masses.

### LIST OF SYMBOLS

$L_j$ -The length of segment j.	$\varphi_{ir}$ -The $i^{\text{th}}$ component of the $r^{\text{th}}$ mode shape.
$S_j(x)$ -The cross-sectional area of the segment j.	$f_i = F^d/N$ -The amplitude of the exciting force in each node, $i = 1, \dots, N$ .
$I_j(x)$ -The squared moment of the segment j.	$\omega_{\text{N-dof-M}}^{*nl}$ -The normalized nonlinear frequency of the N-dof system.
$\rho_j(x)$ -The density of the segment j.	$\chi$ - The taper ratio of the beam.
$E_j(x)$ -The Young's modulus of the segment j.	$x_r$ -The local coordinates in the x-axis, for $r = 1, \dots, N + 2$ .
(N-dof)-N degree of freedom.	$m_r$ - The magnitude of the mass i located at abscissa $x_r$ , for $r = 1, \dots, N$ .
L-The length of SAFGB.	$S_1$ - The cross-sectional area of the section located at $x=0$ .
$\eta_j$ -The normalized mass.	$I_1$ -The squared moment of the section located at $x=0$ .
$A_j$ -The modulus of the displacement $y_j$ of the mass $m_j$ in DB, for $j = 1, \dots, N$ .	$R = \sqrt{I_1/S_1}$ -The radius of gyration of the section located at $x=0$
$a_j$ -The modulus of displacement $y_j$ expressed in MB, for $j = 1, \dots, N$ .	$l_i=L/(N+1)$ -The length of the bar i.
$n$ -The number of add masses.	
$M_i$ -Magnitude of add masses, $i = 1, \dots, n$ .	
$X_i$ -The Coordinate of add masses, $i = 1, \dots, n$ .	
$F^d$ -The intensity of distributed force.	
$F_i$ -The harmonic excitation force applied to node i, $i = 1, \dots, N$	

### 1. INTRODUCTION

In different engineering sectors, such as automotive, and civil engineering, etc. Various structural components are made of stepped or

continuously segmented beams whose physical properties vary from one segment to another, either in the thickness or in the length directions. This last case, is often named axially functional gradient beams and has several advantages and a particular interest in various applications compared to pure or alloyed metals. Treating linear and non-linear, free and forced vibrations of stepped and continuously segmented beam structures made of materials with axial functional gradient SAFGB and containing point masses are rare in the literature, because the differential equations describing them are difficult to solve due to the changing coefficients in these equations. The analytical solution might be impossible to obtain in the case of free and forced vibrations at large displacement. However, few studies that dealt with this kind of problem and used various methods. Mao [1] used the Adomian Decomposition Method (ADM) to study the free vibrations of Euler-Bernoulli beams with multiple cross-sectional steps. Salinic et al [2] proposed a new non-iterative computational technique called the symbolic-numerical method of initial parameters (SNMIP) to deal with the free vibrations of continuously tapered, stepped, and segmented Euler-Bernoulli axial functional gradient beams and rods. Sınır et al [3] addressed free and forced nonlinear vibrations of Euler Bernoulli beams with a non-uniform cross-section. The studied beams are made from axial functional gradient materials. Su et al [4] calculated the linear vibration frequencies of multi-step functional gradient beams and predicted the influence of several parameters on these frequencies, in this study the theoretical model is formulated based on a variation method in conjunction with the first-order shear deformation theory. This work neglected the effect of mass addition on the large displacement dynamic behavior of AFG beams. Adri et al [5] used an analytical approach to calculate the linear and nonlinear vibration frequencies of beams embedded at two ends and carrying masses at different locations. Fakhreddine et al [6] treated the forced vibrations of homogeneous beams carrying various point masses at different positions using a semi-analytical approach.

The objective of the present research is to develop an adaptable discrete model for the large displacement vibrations of SAFGB, subjected to distributed excitation forces and containing point masses at different locations. The beam is modeled by a discrete mechanical system composed by  $N$  masses  $m_r$ ,  $N+2$  spiral springs  $C_r^1$  and,  $N+1$  linear springs  $k_r$ . These components allow finding the expressions of the mass tensor  $m_{ij}$ , the linear stiffness tensor  $k_{ij}$  and the nonlinear stiffness tensor  $b_{ijkl}$  of the  $N$ -dof system modelling the SAFGB. These tensors' numerical values depend on the laws of variation of the mechanical and geometrical properties along the beam length. A discretization is carried out so that the tensors related to each segment are found, and then an assembly is performed that verifies the

compatibility conditions. Due to the discrete nature of this model, the distributed force is replaced by concentric forces on each node. Its values are proportional to the intensity of the applied force and the number of  $N$ -Dof used in the discretization process. Once the formulation is completed, several applications are presented in this study. The linear and non-linear vibration frequencies are calculated using the single mode approach, and compared with others previously published results, which show the applicability of this new model and the validity of the discretisation technique carried out in this study. Details are presented in what follows.

## 2. GENERAL FORMULATION

In this study, a presentation is made of an extension of a discrete mechanical model based on the modal analysis that was presented by Rahmouni, Khnair et Benamar [7]–[9] to investigate the free and excitation forced nonlinear vibrations of inhomogeneous stepped beams carrying point masses in various locations.

### 2.1. Description of the discrete model

For the first time, a discrete model is used to survey the dynamic behavior in the large displacements of a stepped and continuously segmented beam made of a material with an axial functional gradient. Two types of vibrations, free and forced, are treated in this study. We assume that the force  $F^d$  is distributed along the SAFGB. The typical beam and its corresponding discrete model are presented in Fig 1. It was considered that the beam consists of  $R$  segments carrying point masses at different positions. The length, the cross-sectional area, the squared moment, the density and Young's modulus of a segment  $j$  of the beam are noted respectively by,  $L_j$ ,  $S_j(x)$ ,  $I_j(x)$ ,  $\rho_j(x)$ , and  $E_j(x)$ .  $L = \sum_{j=1}^R L_j$  is the total length of the beam.  $\sum_{j=1}^R \beta_j = 1$  and  $\beta_j = L_j/L$  is the ratio between the length  $L_j$  of segment  $j$  and the total length  $L$  of the beam. The equivalent discrete model of SAFGB is composed of  $N$  masses whose magnitude  $m_r$ , for  $r = 1, \dots, N$  simulate the inertia of the beam. The SAFGB carry  $n$  point masses whose magnitude  $M_i$ , and position  $X_i$ , for  $i = 1, \dots, n$ . The bending stiffness of the beam is modeled by  $N+2$  spiral springs of stiffness  $C_r^1$  for  $r = 1, \dots, N+2$ . The geometrical nonlinearity, produced due to large displacement, is modeled by  $N+1$  linear springs of stiffness  $k_r$  for  $r = 1, \dots, N+1$ . The elongation of the linear springs is calculated using the Pythagoras theorem [7]. The total mass of the beam is distributed over the set of  $N$  masses. This distribution is governed by the cross-sectional area's laws of variations, and the density of the segment  $j$ . The elements  $m_r$ ,  $C_r^1$  and  $k_r$  are related to each other as shown in Fig. 1. The values of these elements depend on Young's modulus, density, cross-section geometry, and squared moment of segment  $j$ . The values of these characteristics are

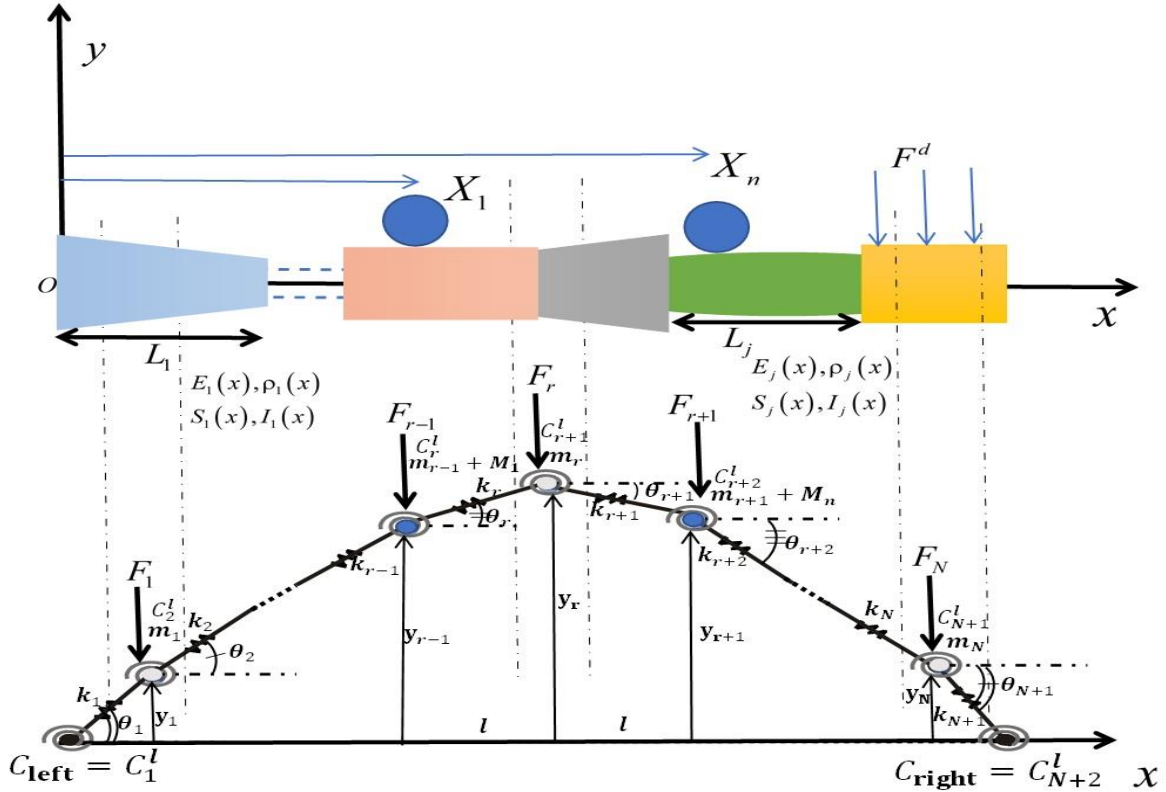


Fig. 1. Typical SAFGB and the corresponding discrete model containing various point masses and subjected to a distributed force

governed by linear, parabolic, exponential or constant laws. Each mass  $m_r$  is simulated by a vertical harmonic force  $F_r$  for  $r = 1, \dots, N$  chosen according to the nonlinear mode to be excited.

The displacement of the mass  $m_r$  is noted by  $y_r$  in displacement basis (DB) and  $\bar{y}_r$  in modal basis (MB) for  $r = 1, \dots, N$ . The displacement vector is then defined by  $\{y\} = y_1 \bar{u}_1 + \dots + y_N \bar{u}_N$  which can also be written as  $\{y\} = \bar{y}_1 \bar{\varphi}_1 + \dots + \bar{y}_N \bar{\varphi}_N$ .  $\{\bar{u}_1, \dots, \bar{u}_r, \dots, \bar{u}_N\}$  is the DB and  $\{\bar{\varphi}_1, \dots, \bar{\varphi}_r, \dots, \bar{\varphi}_N\}$  is the MB. The  $r$ th linear mode shape of the N-Dof System  $\bar{\varphi}_r$  are denoted in DB as  $\bar{\varphi}_r^T = \{\varphi_{1r}, \dots, \varphi_{ir}, \dots, \varphi_{Nr}\}$  for  $r = 1, \dots, N$ .  $\{y_1 \dots y_r \dots y_N\} = [\varphi]^{-1} \{\bar{y}_1 \dots \bar{y}_r \dots \bar{y}_N\}$  where  $[\varphi] = \{[\varphi_{i1}], \dots, [\varphi_{ir}], \dots, [\varphi_{iN}]\}$  is the transition matrix from DB to MB [7], [8].

The system N-Dof presented in Fig 1 is assumed to be subjected to a harmonic excitation force given by the following formula [10]:

$$F_i(t) = f_i \cos(\omega_{NdoF}^n t) = \bar{f}_j \varphi_{ij} \cos(\omega_{NdoF}^n t) \quad (1)$$

$i, j = 1, \dots, N$

$f_i$  and  $\bar{f}_i$  represent the amplitude of the excitation force  $F_i$  applied to the mass  $m_i$  expressed respectively in DB and MB.  $\omega_{NdoF}$  is the excitation frequency of the discrete system.

It is considered that the motion of the system is harmonic according to the law [7], [8], [11], [12]:

$$y_i(t) = A_i \cos(\omega_{NdoF}^n t) = a_j \varphi_{ij} \cos(\omega_{NdoF}^n t) \quad (2)$$

for  $i, j = 1, \dots, N$

$A_i$  is the modulus of displacement  $y_i$  expressed in DB (or the contribution of normalised vector  $\{u_i\}$  of DB), and  $a_j$  is the modulus of displacement  $y_i$  expressed in MB (or contribution of the normalised vector  $\{\varphi_i\}$  of MB [7]).

Using the usual summation convention for the repeated indices  $i, j, k$  and  $l$ , the kinetic, linear and nonlinear potential energies of the N-dof system [7], [8] modelling the SAFGB shown in Fig 1 can be written as:

$$\begin{aligned} T &= \frac{1}{2} \dot{y}_i \dot{y}_j m_{ij}(x_i) = \frac{1}{2} A_i A_j (\omega_{NdoF}^n)^2 m_{ij}(x_i) \sin^2(\omega_{NdoF}^n t) \\ &= \frac{1}{2} a_i a_j (\omega_{NdoF}^n)^2 \bar{m}_{ij}(x_i) \sin^2(\omega_{NdoF}^n t) \quad i, j = 1, N \end{aligned} \quad (3)$$

$$V_l = \frac{1}{2} y_i y_j k_{ij}(x_i) = \frac{1}{2} A_i A_j k_{ij} \cos^2(\omega_{NdoF}^n t) \quad (4)$$

$$= \frac{1}{2} a_i a_j \bar{k}_{ij}(x_i) \cos^2(\omega_{NdoF}^n t) \quad i, j = 1, N$$

$$V_{nl} = \frac{1}{2} y_i y_j y_k y_l b_{ijkl}(x_i) = \frac{1}{2} A_i A_j A_k A_l b_{ijkl}(x_i) \cos^4(\omega_{NdoF}^n t)$$

$$= \frac{1}{2} a_i a_j a_k a_l \bar{b}_{ijkl}(x_i) \cos^4(\omega_{NdoF}^n t) \quad i, j, k, l = 1, \dots, N \quad (5)$$

Where  $m_{ij}$ ,  $k_{ij}$  and  $b_{ijkl}$  respectively ( $\bar{m}_{ij}$ ,  $\bar{k}_{ij}$  and  $\bar{b}_{ijkl}$ ) are the general terms of the mass tensor, the linear tensor and the nonlinear rigidity tensor in DB. (respectively in MB) [7]. The relations between the expressions of this tensors in DB and MB can be

obtained by using the transition matrix  $[\varphi]$  defined earlier in [7]–[10].

$$\bar{m}_{ij} = \varphi_{si} \varphi_{ij} m_{st} \quad (6)$$

$$\bar{k}_{ij} = \varphi_{si} \varphi_{ij} k_{st} \quad (7)$$

$$\bar{b}_{ijkl} = \varphi_{si} \varphi_{ij} \varphi_{pk} \varphi_{ql} b_{stpq} \quad (8)$$

for  $i, j, k, l, s, t, p, q = 1, \dots, N$

The relation between the magnitude of the excitation force in DB and MB can be written as [10]:

$$\bar{f}_i = \Phi_{si} f_s \quad (9)$$

for  $i, s = 1, \dots, N$

The general term of mass tensor is given by the following relation [11], [12]:

$$m_{ij}(x) = m_i(x_i) \delta_{ij} \quad \text{for } i, j = 1, \dots, N \quad (10)$$

$$m_{ij}(x) = \frac{L\rho(x_i)S(x_i)}{N+1} \delta_{ij} \quad (11)$$

for  $i, j = 1, \dots, N$

$\delta_{ij}$  is the Kronecker symbol.

The local coordinates in the x-axis are given by  $x_r = (r-1) \times l$  Fig. 1, for  $r=1, \dots, N+2$ .  $l=L/(N+1)$  is the distance between two successive masses.

If we take into account the  $n$  point masses, we apply a parameter  $\eta_i$  (normalized mass), which is defined as the ratio of the concentric mass' intensity located at the abscissa  $X_i$  and the mass of a homogeneous and uniform beam (also named reference mass) of section  $S_1$  and density  $\rho_1$ . [11] (Related to the cross-section located at  $x=0$ ).

$$\eta_i = \frac{M_i}{L\rho_1 S_1} \quad (12)$$

If we assume that the mass is located at the  $r^{\text{th}}$  position, the  $m_{ij}(x_i)$  is written in this situation as follows:

$$m_{rr}(x_r) = \frac{L\rho(x_r)S(x_r)}{N+1} + \eta_r L\rho_1 S_1 \quad (13)$$

The expression of the potential energy stored in the  $N+2$  spiral springs of the  $N$ -Dof system is given by [7], [11]:

$$V_l = \frac{1}{2l^2} \sum_{r=1}^{N+2} C_r^l (y_r - 2y_{r-1} + y_{r-2})^2 \quad (14)$$

$$y_{N+2} = y_{N+1} = y_0 = y_{-1} = 0$$

When we use the same steps established in [7], we find the  $k_{ij}$  tensor components:

$$k_{rr} = \frac{1}{l^2} (C_r^l + 4C_{r+1}^l + C_{r+2}^l) \quad (15)$$

for  $r = 1, \dots, N$

$$k_{(r-1)r} = k_{r(r-1)} = -\frac{2}{l^2} (C_r^l + C_{r+1}^l) \quad (16)$$

for  $r = 2, \dots, N$

$$k_{(r-2)r} = k_{r(r-2)} = \frac{1}{l^2} C_r^l \quad (17)$$

for  $r = 3, \dots, N$

The elementary potential energy  $dV_{br}$  stored in SAFGB, corresponding to an elementary bar in the continuous beam of length  $dx$ , is given by [7], [11], [12]:

$$dV_{lr} = \frac{1}{2I^3} E_j(x_r) I_j(x_r) (y_r - 2y_{r-1} + y_{r-2})^2 \quad (18)$$

Identifying the two equations (14) and (18), we find the expression of coefficient  $C_r^l$  at the abscise  $x_r$  for the segment  $j$ .

$$C_r^l = \frac{E_j(x_r) I_j(x_r)}{l} \quad \text{for } r = 1, \dots, N+2 \quad (19)$$

To present the nonlinear stiffness tensor corresponding to SAFGB, we use the expression of the energy stored in the  $N+1$  axial spring of stiffness  $k_r$  that models the geometrical nonlinearity due to the large displacement of the beam [7]:

$$V_{nl} = \sum_{r=1}^{N+1} k_r \frac{(y_r - y_{r-1})^4}{8l_r^2} \quad (20)$$

We can rewrite equation (20) for a bar located at abscissa  $x_r$  as follows:

$$V_{nlr} \cong k_r \frac{(y_r - y_{r-1})^4}{8l_r^2} \quad (21)$$

The expression of the stiffness  $k_r$  of the longitudinal spiral spring located at abscissa  $x_r$  for the segment  $j$ , is defined as follows [7], [9]:

$$k_r = \frac{E_j(x_r) S_j(x_r)}{l_r} \quad \text{for } r = 1: N+1 \quad (22)$$

With  $l_1 = l_2 = \dots = l_{N+1} = l$ .

As mentioned in [7], [8]. Equation (20) gives the following expressions of the terms for the nonlinear stiffness tensor that presents the axial load induced in the longitudinal springs by the nonlinear effect:

$$b_{rrrr} = \frac{1}{8l^2} (k_r + k_{r+1}) \quad \text{for } r = 1, \dots, N \quad (23)$$

$$\begin{aligned} b_{rr-1r-1r-1} &= b_{r-1rr-1r-1} = b_{r-1r-1rr-1} \\ &= b_{r-1r-1r-1r} = -\frac{1}{8l^2} k_r \quad \text{for } r = 2, \dots, N \end{aligned} \quad (24)$$

$$\begin{aligned} b_{rrrr-1} &= b_{rrr-1r} = b_{rr-1rr} = b_{r-1rrr} \\ &= -\frac{1}{8l^2} k_r \quad \text{for } r = 2, \dots, N \end{aligned} \quad (25)$$

$$\begin{aligned} b_{rr-1r-1r} &= b_{r-1rr-1r} = b_{r-1r-1rr} \\ &= b_{rr-1rr-1} = b_{r-1rrr-1} = b_{rrr-1r-1} = \frac{1}{8l^2} k_r \\ &\quad \text{for } r = 2, \dots, N \end{aligned} \quad (26)$$

The other values of  $b_{ijkl}$  are equal to zero.

The discretization process is presented as follows.

For segment 1, the coordinate is defined in interval  $0 \leq x \leq L_1$ . The physical and geometrical properties namely Young's modulus, density, cross-sectional area and squared moment are described respectively by the functions  $E_1(x_i)$ ,  $\rho_1(x_i)$ ,  $S_1(x_i)$  and  $I_1(x_i)$  for  $i = 1, \dots, \beta_1(N+1) + 1$ . For segment 2, they are defined in interval  $L_1 \leq x \leq$

$L_1 + L_2$ . These parameters are described by  $E_2(x_i)$ ,  $\rho_2(x_i)$ ,  $S_2(x_i)$  and  $I_2(x_i)$  for  $i = \beta_1(N + 1) + 2, \dots, \beta_1(N + 1) + \beta_2(N + 1) + 1$ . For segment 3 they are defined in interval  $L_1 + L_2 \leq x \leq L_1 + L_2 + L_3$ . These parameters are described by  $E_3(x_i)$ ,  $\rho_3(x_i)$ ,  $S_3(x_i)$  and  $I_3(x_i)$  for  $i = \beta_1(N + 1) + \beta_2(N + 1) + 2, \dots, \beta_1(N + 1) + \beta_2(N + 1) + \beta_3(N + 1) + 1$  and vice versa i.e. applying the same approach to segment j. From the expression of these physical and geometrical parameters, we can find the terms of the tensors for each bar.

**2.2. Amplitude equation for the nonlinear vibration problem**

**2.2.1. General equation**

The nonlinear amplitude equation of the N-Dof system modelling the SAFTB considered is first established using Hamilton’s principle and spectral analysis [5]–[8]:

$$\delta \int_0^{2\pi/\omega} (V_l + V_{nl} - T - F) dt = 0 \quad (28)$$

Replacing T,  $V_l$ ,  $V_{nl}$  and F in this equation by their expressions presented in equations (1) and (3) to (5), integrating the time functions and calculating the derivatives with respect to the  $a_i$ ’s, we obtain a system of nonlinear algebraic equations:

$$3a_i a_j a_k \bar{b}_{ijk} + 2a_i \bar{k}_{ir} - 2a_i \omega^2 \bar{m}_{ir} = \bar{f}_r \quad (29)$$

for  $i, j, k, r = 1, \dots, N$

Which can be written in matrix form as:

$$\frac{3}{2} [\bar{B}(a)] \{a\} + [\bar{K}] \{a\} - (\omega_{N dof}^{nl})^2 [\bar{M}] \{a\} = \{\bar{f}\} \quad (30)$$

Where  $[\bar{M}]$ ,  $[\bar{K}]$ , and  $[\bar{B}(a)]$  are respectively the mass matrix, the linear stiffness matrix and the nonlinear stiffness tensor expressed in the MB and  $\{a\}$  is the displacement vector in the MB.

Equation (29) is a nonlinear equation presenting the nonlinear dynamic behaviour in large displacement of the system N-Dof modelling the SAFTB.

The expression of the  $\omega_{N dof}^{nl}$  parameter nonlinear frequency can be obtained by pre-multiplying Eq. (30) by  $\{a\}^T$  from the left-hand side [7], [8], which leads to the following equation:

$$(\omega_{N dof}^{nl})^2 = \frac{a_i a_j \bar{k}_{ij} + \frac{3}{2} a_i a_j a_k \bar{b}_{ijk}}{a_i a_j \bar{m}_{ij}} - \frac{\bar{f}_i}{\bar{m}_{ij} a_i} \quad (31)$$

**2.2.2 Single Mode approach (SMA)**

The Single mode approach (SMA) is frequently used in the literature [5] and [13] because of the great simplification it brings to the theory, and the little error it causes in the estimation of amplitude dependent nonlinear frequency  $\omega_{N dof}^{nl}$  of the system N-Dof. Applying the SMA to equation (31) leads to:

$$\left( \frac{\omega_{N dof}^{nl}}{\omega_{N dof}^l} \right)^2 = 1 + \frac{3}{2} a_1^2 \frac{\bar{b}_{1111}}{k_{11}} - \frac{\bar{f}_1}{a_1 k_{11}} \quad (32)$$

In which  $k_{11}$ ,  $m_{11}$ ,  $b_{1111}$  and  $f_1$  correspond to the single mode in the neighbourhood of which the nonlinear effect is examined which corresponds to the first mode for the cases considered in this study, were  $\omega_{N dof}^l = \sqrt{k_{11}/m_{11}}$  is the first linear frequency parameter.

**3. RESULT AND DISCUSSION**

In this section, various numerical applications are presented to validate the new approach. The results of linear and nonlinear frequencies are achieved from a program realized by MATLAB software.

**3.1. Validation of the results for the linear case**

We present firstly the results concerning the linear frequencies. In this case, the  $\frac{3}{2} [\bar{B}(a)]$  term is not taken into account, which leads to the following formula:

$$[\bar{K}] \{a\} - (\omega_{N dof}^l)^2 [\bar{M}] \{a\} = 0 \quad (33)$$

The **eig** function integrated in MATLAB software is used to find the linear vibration frequencies  $\omega_{N dof r}^l$  for  $r = 1$  to  $N$ , corresponding to the  $N$  vibration modes of the discrete system modelling the SAFTB.

Two numerical applications are presented in this study, the first one corresponds to a beam with three steps. The second one corresponds to a beam composed of two segments continuously attached.

**3.1.1. Example 1**

The example shown in [2], corresponds to a beam consisting of four segments for rectangular cross-section. The geometrical characteristics of the corresponds beam are:  $\beta_1 = 0.25$ ,  $\beta_2 = 0.30$ ,  $\beta_3 = 0.25$  and  $\beta_4 = 0.20$ .  $S_2/S_1 = 0.8$ ,  $S_3/S_1 = 0.65$ ,  $S_4/S_1 = 0.25$ , the width of this beam is assumed to be constant. Two types of beams are considered in this example, the first one corresponds to a homogeneous beam with Young’s modulus and mass density assumed constant i.e.,  $E(x) = E_{Al}$  and  $\rho(x) = \rho_{Al}$  for  $0 \leq x \leq L$  (Material 1). The second beam corresponds to an axial functional gradient beam with  $E(x) = E_{Al}(1 + (E_{Al}/E_{Zr} - 1)(x/L)^2)$  and  $\rho(x) = \rho_{Al}(1 + (\rho_{Al}/\rho_{Zr} - 1)(x/L)^2)$  for  $0 \leq x \leq L$  (Material 2). It is considered that the axial functional gradient material is composed of two constituents, zirconia ZrO2 and aluminum Al, whose mechanical characteristics are presented in Table 1.

Table 2 presents the first 10 dimensionless linear frequencies  $\sqrt{\omega_{N dof r}^{*l}} = \sqrt{\omega_{N dof r}^l \sqrt{L^4 S_1 \rho_{Al} / I_1 E_{Al}}}$  estimated with  $N=123$  and for the three boundary conditions, (Embedded-Embedded) (E-E),  $C_1^l = C_{N+2}^l = \infty$ , (Simply-Supported) (S-S),  $C_1^l =$

$C_{N+2}^l = 0$  and (Embedded-Supported) (E-S),  $C_1^l = \infty$  and  $C_{N+2}^l = 0$ . It is already known in the literature that the results obtained for the linear case by this discrete model are improved by increasing the N-Dof [7], [8].

From the results presented in Table 2, it can be seen that the use of material 2 instead of material 1 results in a decrease in all frequency values for the S-S and E-E boundary conditions. For the C-S boundary condition, it can be seen that the

frequencies related to material 2 are low compared to material 1, except for the second frequency where the opposite is observed.

Table 1. The values of the young's modulus and density

	Young's modulus (N/m <sup>2</sup> )	Density (Kg/m <sup>3</sup> )
Al (Aluminium)	$E_{Al} = 70 \times 10^9$	$\rho_{Al} = 2702$
Zr (Zirconia)	$E_{Zr} = 200 \times 10^9$	$E_{Zr} = 5700$

Table 2. Comparison of the six dimensionless frequencies with the results given in [2] related the beam presented in section 3.3.1

$\sqrt{\omega_{Ndof r}^{*l}}$	Material	S-S		E-E		E-S	
		Present study	[2]	Present study	[2]	Present study	[2]
$\sqrt{\omega_{Ndof1}^{*l}}$	1	2.2421	2.24074	3.5447	3.54196	3.0324	3.02686
	2	2.0880	2.08694	3.4076	3.4077	2.99914	3.00028
$\sqrt{\omega_{Ndof2}^{*l}}$	1	4.6346	4.63823	5.8188	5.81163	5.4161	5.42184
	2	4.6241	4.62467	5.7280	5.72338	5.4256	5.43323
$\sqrt{\omega_{Ndof3}^{*l}}$	1	7.4301	7.43284	8.4859	8.48187	8.1161	8.10836
	2	7.3803	7.38797	8.3909	8.39335	8.0493	8.04824
$\sqrt{\omega_{Ndof4}^{*l}}$	1	9.9365	-----	11.3432	-----	10.3846	-----
	2	9.6956	-----	11.1432	-----	10.0815	-----
$\sqrt{\omega_{Ndof5}^{*l}}$	1	11.8066	-----	13.1543	-----	12.4916	-----
	2	11.5999	-----	12.8529	-----	12.3061	-----
$\sqrt{\omega_{Ndof6}^{*l}}$	1	14.6163	-----	15.7312	-----	15.3828	-----
	2	14.4182	-----	15.4894	-----	15.1504	-----

Table 3. Comparison of the six dimensionless frequencies related the beam presented in section 3.3.2 with the results given in [2]

$\sqrt{\omega_{Ndof r}^{*l}}$	Material	$\chi = 0.1$ $\beta_1 = 0.2$		$\chi = 0.1$ $\beta_1 = 0.4$		$\chi = 0.2$ $\beta_1 = 0.2$		$\chi = 0.3$ $\beta_1 = 0.2$		$\chi = 0.4$ $\beta_1 = 0.4$	
		Present study	[2]								
$\sqrt{\omega_{Ndof1}^{*l}}$	1	4.1654	4.16752	3.2999	3.29393	4.0445	4.04916	3.8675	3.8675	3.3932	3.3932
	2	4.2706	4.27377	3.3864	3.38057	4.1185	4.11449	3.9022	3.9022	3.4082	3.4082
$\sqrt{\omega_{Ndof2}^{*l}}$	1	11.8038	11.7968	9.1456	9.14226	9.3114	9.31172	8.2888	8.2888	7.3329	7.3329
	2	11.6069	11.6037	9.1022	9.10021	9.1525	9.15617	8.1503	8.1503	7.2296	7.2296
$\sqrt{\omega_{Ndof3}^{*l}}$	1	11.6831	16.6743	14.6747	14.6626	13.8233	13.8225	12.4168	12.4168	10.9214	10.9214
	2	16.4580	16.4543	14.4562	14.4473	13.6117	13.6158	12.2198	12.2198	10.7482	10.7482
$\sqrt{\omega_{Ndof4}^{*l}}$	1	21.8975	-----	18.6625	-----	18.2714	-----	16.5012	16.5012	14.5917	14.5917
	2	21.5979	-----	18.3728	-----	17.993	-----	16.2520	16.2520	14.3607	14.3607
$\sqrt{\omega_{Ndof5}^{*l}}$	1	27.3501	-----	23.3775	-----	22.7516	-----	20.6555	20.6555	18.1953	18.1953
	2	27.0055	-----	23.0908	-----	22.4166	-----	20.2609	20.2609	17.9183	17.9183
$\sqrt{\omega_{Ndof6}^{*l}}$	1	32.6299	-----	27.8282	-----	27.2940	-----	24.6575	24.6575	21.8393	21.8393
	2	32.2342	-----	27.4473	-----	26.9003	-----	24.2937	24.2937	21.5032	21.5032

**3.1.2. Example 2**

In this example, a simply supported beam formed by two continuously attached elements is considered. The width is supposed to be constant,  $b_1(x) = b_2(x) = b_1$  for  $0 \leq x \leq L$  and the thickness is assumed to be variable according to the following laws:

$$h_1(x) = h_1 \quad \text{with } 0 \leq x \leq L\beta_1$$

For the segment 1

$$h_2(x) = h_1 \left[ 1 + \frac{1-\chi}{\chi L(1-\beta_1)}(x-\beta_1 L) \right] \quad \text{with } \beta_1 L \leq x \leq L$$

For the segment 2

$\chi$  is the taper ratio of the thickness, and  $\beta_1$  is the length ratio related to the first segment.

Table 3 shows a comparison of the results of the frequencies of the considered beam with the results of [2] for different values of  $\chi$  and  $\beta_1$  according to material 1 and 2. It can be seen that the agreement with [2] is excellent.

The results of the dimensional frequencies related to the two examples presented above are in a good agreement with those published in [2] by increasing the value of N-Dof .

**3.2. Validation of results for the free nonlinear case**

The example presented in this section is the one examined in [14]. It is a beam consisting of two homogeneous segments continuously attached to each other. Two configurations are possible, the first one concerns a beam of a constant width and a variable thickness that is named beam A. The second one corresponds to a beam of a constant thickness and a variable width, named beam B.

The area of the cross-section and the squared moment of each segment are given by the following relationships:

$$\begin{cases} S_1(x) = S_0 \left( 1 + \chi \left( \frac{2x}{L} \right) \right) \\ I_1(x) = I_0 \left( 1 + \chi \left( \frac{2x}{L} \right) \right)^n \end{cases} \quad -\beta_1 L \leq x \leq 0$$

For the segment 1

$$\begin{cases} S_2(x) = S_0 \left( 1 - \chi \left( \frac{2x}{L} \right) \right) \\ I_2(x) = I_0 \left( 1 - \chi \left( \frac{2x}{L} \right) \right)^n \end{cases} \quad 0 \leq x \leq \beta_1 L$$

For the segment 2

With  $\chi$  being the taper ratio of the beam,  $\beta_1$  is the ratio of the lengths.  $n=3$  corresponds to Beam A, and  $n=1$  corresponds to Beam B. The two segments have the same length i.e.  $\beta_1 = 0.5$ .

The results are illustrated in the form of backbone curves obtained by plot equation (32) for two boundary condition, E-E and S-S and for different values of N-Dof. In these curves, the abscissa axis presents the ratio between the first nonlinear and linear dimensionless frequencies

$\omega_{N\text{dof}}^{*nl} / \omega_{N\text{dof}}^{*l}$  and the ordinate axis presents the maximum nondimensional amplitude  $A_{max}^*$  defined by  $A_{max}^* = A_{max} / R$  with  $R = \sqrt{I_1 / S_1}$  being the radius of gyration of the section located at  $x=0$ . in this example we take  $f_i=0$ .

Fig 2-a;2-b and 3 show a comparison of the backbone curves of the present study with that presented in [14] respectively for SS and EE boundary conditions and for different values of N-Dof.

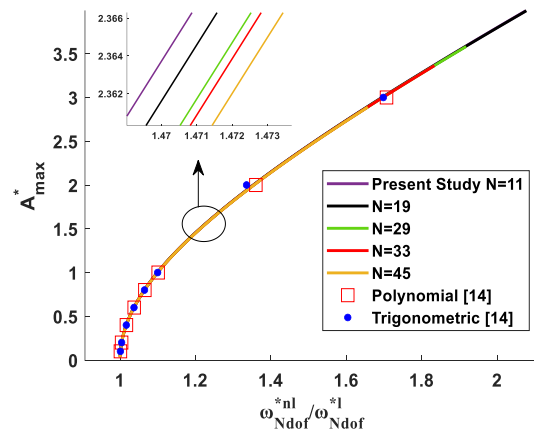


Fig. 2-a. Comparison of the backbone curves for S-S beam A with the results published in [14] for  $\chi = 0.4$

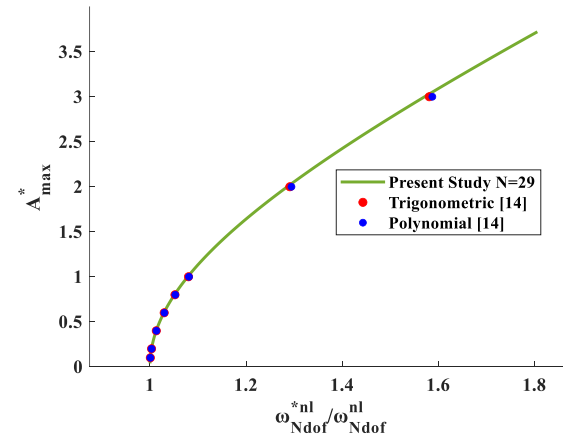


Fig. 2-b. Comparison of the backbone curves for S-S beam B with the results published in [14] for  $\chi = 0.4$

It can be seen that the convergence obtained by the discrete model with 11, 19, 29, 33 and 45 N-Dof is practically stable, i.e., almost independent of the number of N-Dof. It can be concluded that it is not necessary to use a higher number of N-Dof [7], since for N=29 for example the curves obtained of the present study converge well to the published results [14] for beam A, and B and for the two boundary conditions E-E and S-S.

It is clear from Fig 3 that as the taper ratio  $\chi$  is increased, the nonlinearity becomes more significant and the expected hardening effect is observed.

It should be noted that in the following we keep the number of N-dof at the value  $N=29$ , it allows to have good results and a minimum time of execution for MATLAB.

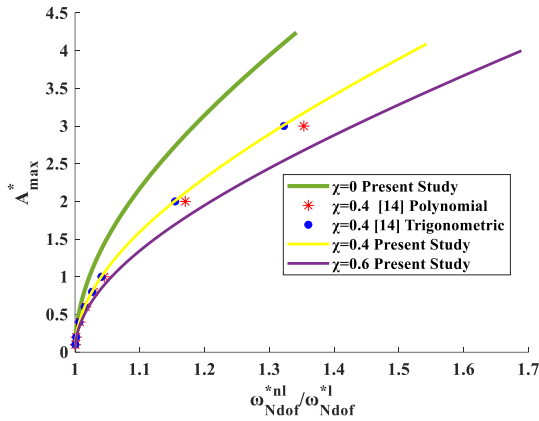


Fig. 3. Comparison of the backbone curves for E-E beam A with the results published in [14] for various values of  $\chi$

### 3.3. Results for the forced nonlinear case (homogeneous beam)

In this section, we present the results of the nonlinear vibration frequencies and the corresponding maximum amplitude in the forced case. The force distribution was chosen to stimulate the first mode, which is considered predominant in this study. The values of the excitation amplitude  $f_i$  of each force  $F_i = f_i \cos(\omega_{Ndof}^{nl} t)$  in DB are given by  $f_i = \varphi_{i1} f$ , [10].  $\varphi_{i1}$  being the  $i^{\text{th}}$  component of the first mode shape, and  $f$  is the amplitude of the exciting force which is defined as the total force distributed over the SAFGB divided by the number of masses N-Dof chosen in the discretization process i.e.  $f = F^d/N$ .

Fig 4 shows the plot of equation (32), which present the response in non-linear and linear frequency ratio as a function of the maximum dimensionless amplitude in the vicinity of the first mode, which is related to the beam presented in section 3.2 with a taper ratio equal to  $\chi = 0.4$ . The beam considered is assumed to be excited by a distributed force  $F^d=100$ .

The non-linear hardening effect and the multi-value zones in which the jump phenomenon can arise, can be more clearly identified.

Fig 5 shows the non-linear frequency response curves for beam A for  $\chi = 0.4$  that is excited by different values of the force distributed along the length of the beam. It can be observed that the variation of the exciting force's intensity affects the curve.

Figs 6 and 7 respectively show the effect of the geometric non-linearity as a function of the taper ratio  $\chi$  of beam A and B for  $F^d=800$ . It can be seen that the hardening effect increases with  $\chi$  for beam A and is approximately stable for beam B.

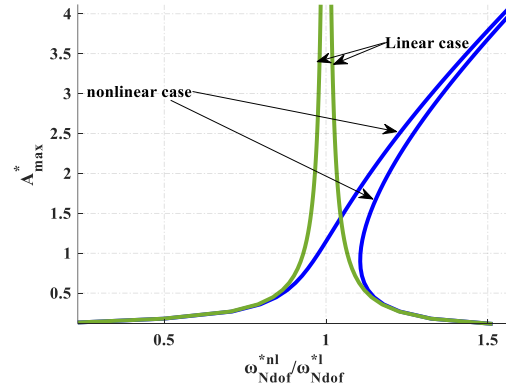


Fig. 4. Linear and nonlinear frequency response for E-E beam A with  $\chi = 0.4$  and  $F^d=100$

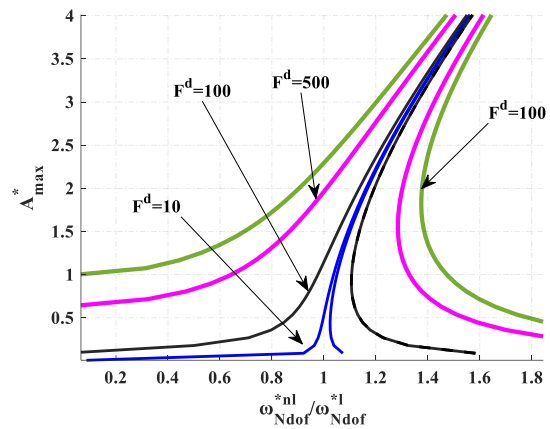


Fig. 5. Comparison of the nonlinear frequency's response for E-E beam A with  $\chi = 0.4$  for different values of  $F^d$

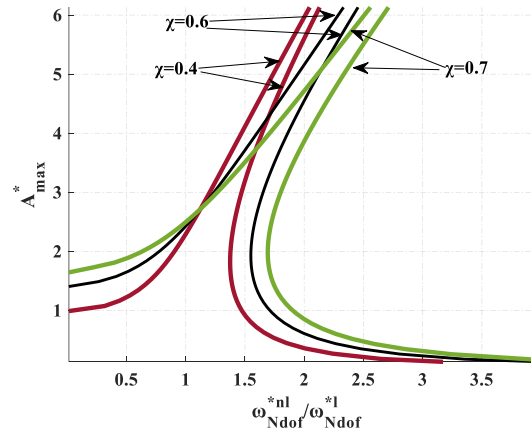


Fig. 6. Comparison of the nonlinear frequency's response for E-E beam A for different values of  $\chi$  and  $F^d=800$

Fig 8 shows the effect of the boundary conditions on the frequency response of beam A for  $\chi=0.6$  and for  $F^d=500$ . It can be seen from Fig 8 that the hardening effect is significant for the S-S boundary conditions compared to the E-E boundary conditions.

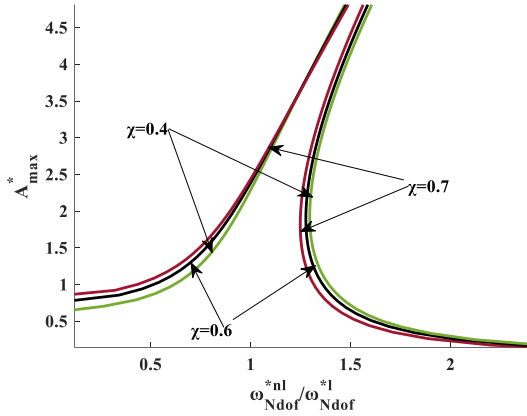


Fig. 7. Nonlinear frequency response for E-E Beam B for different values of  $\chi$  and for  $F^d=800$

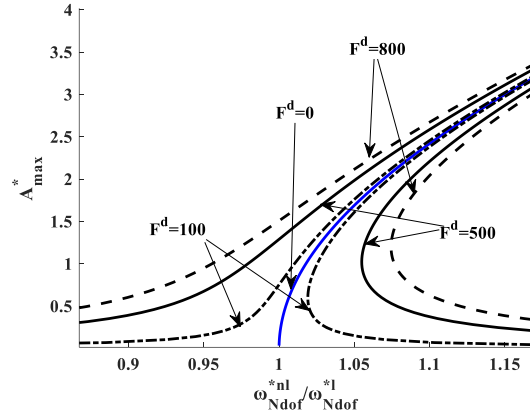


Fig. 9. Comparison of nonlinear frequency response for E-E beam, with  $\beta_2 = 0.25$  and for different values of  $F^d$

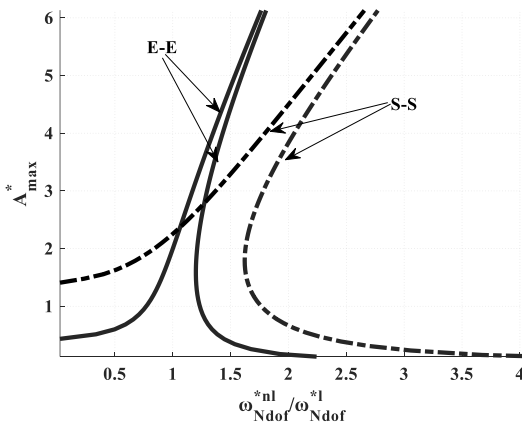


Fig. 8. The effect of boundary conditions on the frequency response related to beam A for  $\chi = 0.6$  and for  $F^d=500$

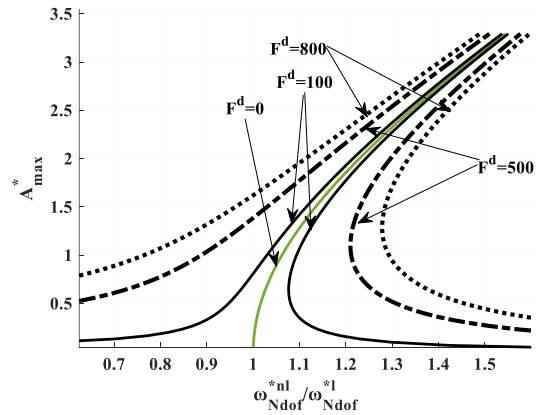


Fig. 10. Comparison of nonlinear frequency response for S-S beam, for  $\beta_2 = 0.25$  and for different values of  $F^d$

### 3.4. Results for the nonhomogeneous beam in free and forced case

Considering two-step beam of length  $L=1m$  according to material 2 presented in section 3.1.1. The beam is subjected to a distributed force of intensity  $F^d$ . The geometrical characteristics are given by:  $\beta_1 = 0.375$ ,  $\beta_2 = 0.25$  and  $\beta_3 = 0.375$ .  $S_2/S_1 = 0.6$ ,  $S_3/S_1 = 1$ . Fig 9 and 10 show respectively the nonlinear frequency response for E-E and S-S boundary condition, and for different values of excitation  $F^d$ . Fig 11 shows the nonlinear frequency response of the S-S beam for different values of  $\beta_2$  and for  $F^d=500$ . In this example, if we take  $\beta_2$  as a controlling parameter, the values of  $\beta_1$  and  $\beta_3$  are calculated as follows:  $\beta_1 = \beta_3 = (1 - \beta_2)/2$ .

For Figs 9, 10 and 11, we can see that the non-linearity is always of the hardening type. When we change the value of the force distributed on the beam, the frequency response also changes. We can clearly see on the right side of Fig 11 that there is a jump phenomenon, and an increase of the  $\beta_2$  coefficient leads to an increase of the frequency for a fixed value of the amplitude.

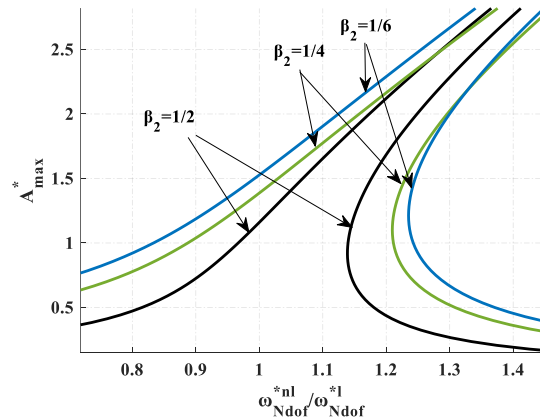


Fig. 11. The effect of the change in  $\beta_2$  on the frequency response for S-S boundary condition and for  $F^d=500$

### 3.5. Results for the nonhomogeneous beam in free and forced case containing various point masses

In order to validate the results of the present study for the Stepped AFG beams containing point masses, a comparison was performed with the results published in [15] for a homogeneous and uniform beam carrying 3 point masses respectively at  $X_i = (X_1 = 0.2; X_2 = 0.5; X_3 = 0.7)$  and magnitude  $\eta_i =$

( $\eta_1 = 10; \eta_2 = 10; \eta_3 = 10$ ). The results are presented as backbone curve given in Fig 12 whose abscissa axis matches the normalized nonlinear frequency  $\omega_{N\text{dof-M}}^{\text{nl}} = \omega_{N\text{dof-M}}^{\text{nl}} L^2 \sqrt{\rho_{Al} S_1 / I_1 E_{Al}}$  and the ordinate axis corresponds to the normalized maximum amplitude  $A_{\text{max}}^*$ .  $\rho_{Al}, S_1, I_1$  and  $E_{Al}$  are the geometrical and physical characteristics of the uniform beam.

Fig 13 illustrates the backbone curve for the SAFGB presented in section 3.4 for  $\beta_2 = 0.2$  and corresponds to material 2, carrying 2-point masses respectively at  $X_i = (X_1 = 0.1; X_2 = 0.7)$  and magnitude  $\eta_i = (\eta_1 = 1; \eta_2 = 1)$ .

It can be seen that the effect of non-linearity increases or decreases by varying the position, the number and the magnitude of the masses added to the beam and the nature of the material used.

Fig 14 illustrates the forced frequency response related to the beam presented in section 3.4 corresponds to material 2 for  $\beta_2 = 0.2$  and carrying two-point masses at  $X_i = (X_1 = 0.1; X_2 = 0.7)$  and magnitude  $\eta_i = (\eta_1 = 10; \eta_2 = 10)$ .

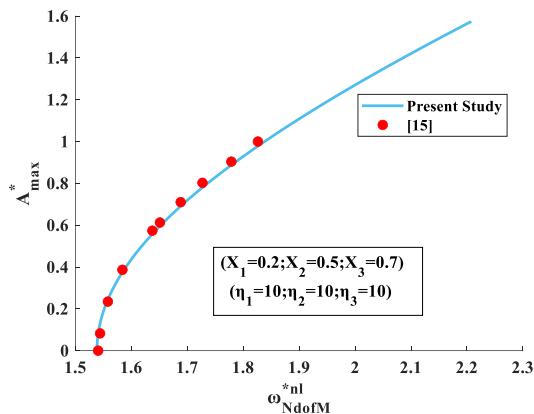


Fig. 12. Comparison of nonlinear frequency response with the results published in [15] for the beam containing point masses

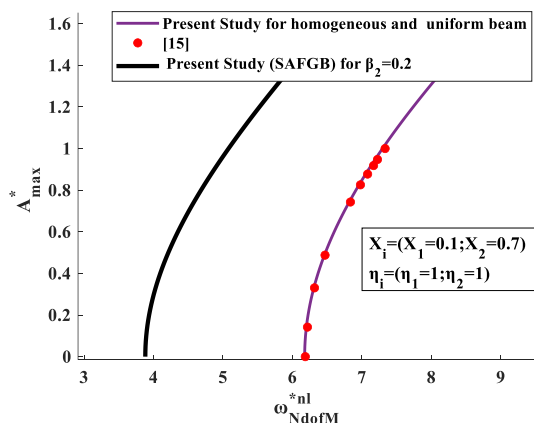


Fig. 13. The effect of the Number of point masses and the nature of beam on nonlinear frequency response for S-S boundary condition

#### 4. CONCLUSION

In this work, we have examined the free and forced vibration at large amplitude of SAFGB

containing added point masses at different locations. The results found of the dimensionless frequencies in the linear and nonlinear cases using the single mode approach are in good agreement with other previously published data, which shows the reliability of this new model. These results of the nonlinear dimensionless frequencies for beams containing point masses have been first compared to other results for the homogeneous beam. For the SAFGB, no previous results were found in literature. This model allows the prediction of large amplitude vibration frequencies for any types of Stepped beam carrying point masses, and for any combination of functional gradient materials.

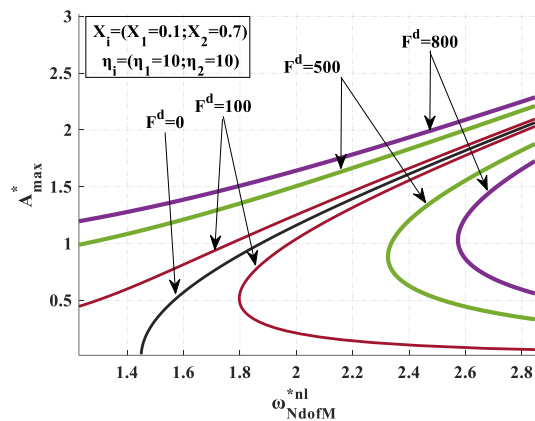


Fig. 14. The effect of the values of  $F^d$  on nonlinear frequency response for S-S boundary condition

**Author contributions:** research concept and design, A.M.; Collection and/or assembly of data, A.M.; Data analysis and interpretation, A.M; Writing the article, A.M; Critical revision of the article, A.R., O.B., R.B.; Final approval of the article, A.R., O.B., R.B.

**Declaration of competing interest:** The authors declare that they have no known competing financial interests or personal relationships that could have appeared to influence the work reported in this paper.

#### REFERENCES

1. Mao Q. Free vibration analysis of multiple-stepped beams by using Adomian decomposition method. *Mathematical and Computer Modelling*. 2011;54(1–2):756–764. <https://doi.org/10.1016/j.mcm.2011.03.019>.
2. Šalinić S, Obradović A, Tomović A. Free vibration analysis of axially functionally graded tapered, stepped, and continuously segmented rods and beams. *Composites Part B: Engineering*. 2018; 150:135–143. <https://doi.org/10.1016/j.compositesb.2018.05.060>.
3. Sımr S, Çevik M, Sımr BG. Nonlinear free and forced vibration analyses of axially functionally graded Euler-Bernoulli beams with non-uniform cross-section. *Composites Part B: Engineering*. 2018;148: 123–131. <https://doi.org/10.1016/j.compositesb.2018.04.061>.
4. Su Z, Jin G, Ye T. Vibration analysis of multiple-stepped functionally graded beams with general boundary conditions. *Composite Structures*.

- 2018;186:315–323.  
<https://doi.org/10.1016/j.compstruct.2017.12.018>.
5. Adri A, Benamar R. Linear and geometrically non-linear frequencies and mode shapes of beams carrying a point mass at various locations. an analytical approach and a parametric study. *Diagnostyka*. 2017; 18(2):2-9.
  6. Fakhreddine H, Adri A, Chajdi M, Rifai S, Benamar R. A multimode approach to geometrically non-linear forced vibration of beams carrying point masses. *Diagnostyka*. 2020;21(4):23–33.  
<https://doi.org/10.29354/diag/128603>.
  7. Rahmouni A, Beidouri Z, Benamar R. A discrete model for geometrically nonlinear transverse free constrained vibrations of beams with various end conditions. *Journal of Sound and Vibration*. 2013;332(20):5115–5134.  
<https://doi.org/10.1016/j.jsv.2013.04.011>.
  8. Khnajar A, Benamar R. A discrete model for nonlinear vibrations of a simply supported cracked beams resting on elastic foundations. *Diagnostyka*, 2017;18(3):2-8.
  9. Rahmouni A, Benamar R. A homogenization procedure and a physical discrete model for geometrically nonlinear transverse vibrations of a clamped beam made of a functionally graded material. *Diagnostyka*. 2017; 18(3):2-7.
  10. Eddanguir A, Beidouri Z, Benamar R. Geometrically nonlinear transverse steady-state periodic forced vibration of multi-degree-of-freedom discrete systems with a distributed nonlinearity. *Ain Shams Engineering Journal*. 2012;3(3):191–207.  
<https://doi.org/10.1016/j.asej.2012.03.007>.
  11. Moukhliiss A, Rahmouni A, Bouksour O, Benamar R. Using the discrete model for the processing of natural vibrations, tapered beams made of aFG materials carrying masses at different spots. *Materials Today: Proceedings*. 2022;52:21–28.  
<https://doi.org/10.1016/j.matpr.2021.10.107>.
  12. Moukhliiss A, Rahmouni A, Bouksour O, Benamar R. N-dof discrete model to investigate free vibrations of cracked tapered beams and resting on winkler elastic foundations. *International Journal on Technical and Physical Problems of Engineering*. 2022;14(1):1-7.
  13. Merrimi El, El Bikri K, Benamar R. Geometrically non-linear steady state periodic forced response of a clamped-clamped beam with an edge open crack. *Comptes Rendus Mécanique*. 2011;339(11):727–742.  
<https://doi.org/10.1016/j.crme.2011.07.008>.
  14. Raju KK, Shastry BP, Rao GV. A finite element formulation for the large amplitude vibrations of tapered beams. *Journal of Sound and Vibration*. 1976;47(4):595–598. [https://doi.org/10.1016/0022-460x\(76\)90887-7](https://doi.org/10.1016/0022-460x(76)90887-7).
  15. Özkaya E. Non-linear transverse vibrations of a simply supported beam carrying concentrated masses. *Journal of Sound and Vibration*. 2002;257(3):413–424.  
<https://doi.org/10.1006/jsvi.2002.5042>.



**Anass MOUKHLISS** was born in Casablanca, Morocco, 1995. He received the Master in mechanical-energy in 2018, University Hassan II of Casablanca, Morocco, and Ph.D student at the National Higher School of Electricity and Mechanics, (ENSEM), Hassan II University of Casablanca, and member of the 'Mechanics, Production and Industrial Engineering' LMPGI laboratory, His research interest is in mechanical engineering, and Numerical modeling of structures.



**Abdellatif RAHMOUNI** was born in Berrechid, Morocco, 1963, Professor of Mechanical Engineering at the Superior School of Technology (EST) - University Hassan II of Casablanca, Morocco. He got his engineering degree in Design and Mechanical Manufacturing, 1989, and Ph.D. degrees of Applied Science, Specialty: Simulation, Instrumentation and Measurement in 2015 from the Mohammadia School of Engineers (EMI) - Mohammed V University of Rabat, Morocco, His research interest is in mechanical engineering, Numerical modeling of structures.



**Otmane BOUKSOUR** was born in Rabat, Morocco, 1957. He received the Eng. Degree in Civil Engineering from Mohammadia School of Engineers, University Mohamed V of Rabat (Rabat, Morocco) in 1981 and the M.Sc. and Ph.D. degrees in Structures and Mechanic of Solids from University of Sherbrooke (Quebec, Canada) in 1986 and 1990, respectively. Currently, he is a Professor in Mechanical Engineering Department at High School of Technology, University Hassan II of Casablanca (Casablanca, Morocco). His research interest is in Industrial Engineering, Logistics and Numerical modeling of structures.



**Rhali BENAMAR** was born in Fes, Morocco, 1960, Professor of Mechanical Engineering and Vibrations at the Mohammadia School of Engineering (EMI) - Mohammed V University of Rabat, Morocco. He got his engineering degree in civil engineering in 1982 from the 'Ecole Nationale des Ponts et Chaussées' of Paris, France. He received his Ph.D. in 1990 from the Institute of Sound and Vibration at the University of Southampton, United Kingdom His research interest is in mechanical engineering, Numerical modeling of structures, gave lectures at NASA in 1998 and Honored in 2006, one of the journal of sound and vibration's most cited authors.

Received 2022-08-13

Accepted 2022-10-06

Available online 2022-10-14